Research Article

Journal of Environmental Nanotechnology

# Design, Simulation, and Analysis of S-shaped Nanobeam-based Multi-directional Inertial Sensor

Mohammad Taj[1*], N. V. R. G. Vikram[2], Veda Sandeep Nagaraja[3] and G. Nithya[4]

[1]Department of Electronics and Communication Engineering, Aditya University, Surampalem, AP, India
[2]Department of Electronics and Communication Engineering, Vignan's Foundation for Science, Technology & Research, Guntur, AP, India
[3]Tyndall National Institute, University College Cork, Cork, Ireland
[4]Department of Electronics and Communication Engineering, Nitte Meenakshi Institute of Technology, Yelahanka, Bengaluru, AP, India
Received: 21.06.2025 Accepted: 31.07.2025 Published: 30.09.2025
*mdtaj405@gmail.Com

## ABSTRACT

Inertial sensors are used to measure the change of momentum along with the applied acceleration force across various applications, such as biomedical, defense, automobile, and robotics. Accelerometers and gyroscopes, together, constitute inertial sensors. Over the past few decades, these sensors have been widely used for several engineering applications. This work proposes a Micro-Electro-Mechanical Systems (MEMS)-based device for sensing inertia. The designed structure incorporates a proof mass to measure displacements caused by inertial forces during linear and rotational motion, making it a candidate for patenting. The designed structure employs proof mass, which could be used to measure displacements due to inertia under linear and rotational moments, which can be patented. Modelling and simulations of the sensor are carried out using COMSOL Multiphysics® software. Multi-physics simulations are carried out on the model to evaluate the device's performance under applied linear and angular momentum. The sensor demonstrates high sensitivity, as shown in the simulation results. Finally, the efficacy of the inertial sensor and its potential for future improvements are discussed.

**Keywords:** MEMS; COMSOL Multiphysics®; Accelerometer; Inertial sensor; Multi-directional.

## 1. INTRODUCTION

The MEMS (Micro-Electro-Mechanical Systems) era has led to applications in multidisciplinary domains like motors, industries, and biomedical (Collin *et al.* 2013). MEMS-based accelerometers are employed to quantify the alternation in inertia of the shifting object, in addition to the effect, through mechanical or electromechanical measurements (Camomilla *et al.* 2018). Accelerometers detect inertia in a wide variety of packages, inclusive of automobile airbag structures, accident alerting structures, mobile telephones, commercial operations, army applications, and biomedical programs (Kou *et al.* 2017; Mahmood *et al.* 2015).

Aydemir and Atkin (2015) have designed a three-axis inertial measurement unit, but the size of the sensor was very large. The proof mass of this sensor is spanning over an area of 4 $mm^2$. Due to this size, sensitivity becomes very low (Edalatfar *et al.* 2016).

According to Hsu *et al.* (2009), measurement of the acceleration in the z-direction is a main challenge for the sensor. In most of the designs, they included a separate sensor that measures the acceleration in the z-path, which makes the thickness of the sensor excessive, whilst sensors are piling in the vertical direction (Solanki *et al.* 2011).

The important specification for the inertial sensor is capacitive sensitivity, and it needs to be as high as possible. The change in capacitance relative to the applied acceleration is called sensitivity. The size is inversely proportional to the sensitivity; with the increase in dimensions, the sensitivity decreases (Young *et al.* 2012).

The proposed architecture will be especially advantageous for applications necessitating the detection of multi-directional inertia. The proof mass exhibits angular or linear movement when subjected to external momentum (Ahmed *et al.* 2012). The relative displacement/area between the electrodes in the device is modified due to the movement. This results in a variation in capacitance, which is subsequently utilized to measure acceleration (Taj *et al.* 2022). The angular acceleration will be ascertained by employing a correlation between the variation in capacitance and the angular momentum (Hsu *et al.* 2009). This study will examine the measurement of rotational acceleration, capacitance estimates, and stress analysis concerning rotational inertia. The suggested sensor can measure both linear and angular acceleration. Linear and angular displacements are often quantified utilizing various sensors within the system. The proposed sensor may resolve integration issues and decrease both cost and space (Chae *et al.* 2005).

This research presents a new MEMS-based sensor capable of multi-directional inertial measurement, which shows improved sensitivity and accuracy in motion detection. Optimized proof mass configuration in the design reduces cross-axis sensitivity while maintaining strong performance capabilities (Lemkin *et al.* 1997). Multi-physics simulations, such as mechanical, electrostatic, and thermal analyses, were conducted using COMSOL Multiphysics® to verify functionality. The proposed sensor achieves better displacement sensitivity along with improved signal-to-noise ratio compared to traditional models (Rudolf *et al.* 2014). The sensor finds use in automotive and aerospace fields and extends its applications to biomedical and industrial motion tracking, along with scalable solutions for wearable and robotic technologies (Aruna *et al.* 2025). Standard microfabrication processes align with this design to support extensive production capabilities and future sensing technology development (Krishnan *et al.* 2007).

MEMS inertial sensors are used in many industries, like navigation for planes, defense, and self-driving cars, as well as car safety systems like airbags. They are also found in consumer gadgets for motion tracking in phones and game controllers, and in medical devices for prosthetics and therapy (Xiong *et al.* 2005). The sensor has a proof mass that shifts when forces act on it. This movement is measured through capacitive or piezoresistive methods to turn it into an electrical signal. COMSOL Multiphysics® simulations showed a high displacement sensitivity of 821.9241 fF/g, and eigen frequency tests found a resonance frequency of 42 kHz, which helps in accurate motion detection. Furthermore, thermal and structural tests indicated reliability in different environmental situations, confirming the sensor's dependability for practical use.

## 1.1 Size Effects in MEMS Sensors

Optimizing the size of a MEMS sensor is a key challenge in improving its performance. Design of MEMS sensors takes into consideration the effects of size on their mechanical and electro-mechanical processes as well as their functioning. Unlike macro-scale systems, MEMS systems behave differently because of the high surface-to-volume ratio, changes in material properties, and quantum-level interactions. MEMS devices modeling and design would not be accurate without a rational approach to these phenomena, which are dependent on size (Benmessaoud and Nasreddine, 2013).

### 1.1.1 Surface Effect

Another effect is that as the dimensions of structures shrink, surface-based effects such as surface stress, adhesion, and friction become more significant. Surface force effects below the surface influence the mechanical behavior of MEMS devices and the stiffness, strength, and reliability that they can achieve (Geeri *et al.* 2023). To illustrate, as surface energy tension becomes prominent, Young's modulus may change at the micro-scale, making structures either less stiff or more stiff than bulk structures, leading to more compliance (Wenk *et al.* 2024).

### 1.1.2 Material Property Variations

Changes to grain structures, defects, and dislocation movement all contribute to the difference between micro-sized material properties and their bulk values (Kumaran *et al.* 2023). Due to the existence of residual stresses and the interaction of grain boundaries and interfaces, thin films employed in MEMS devices often exhibit mechanical properties that differ from those of bulk materials. Experimental data suggest that thinner films have increased yield strength and hardness due to dislocation confinement and the Hall-Petch effect (Marzencki *et al.* 2007).

### 1.1.3 Electrostatic and Casimir Effects

MEMS actuation and sensing are challenged at smaller scales due to the dominance of electrostatic forces over inertial and gravitational forces. MEMS devices can experience unintentional stiction, and pull-in instability due to the impact of static forces which can dramatically affect the productivity and reliability of the device (Kwon *et al.* 2000). Moreover, quantum vacuum oscillations give rise to Casimir forces at the nano-scale, which can cause attractive forces between components that are closely spaced and can lead to device failure (Shen *et al.* 2009).

### 1.1.4 Scaling Laws and Modeling Approaches

The aging scaling laws for MEMS systems' behavior need to be updated in order to account for the size-relevant factors. Classical models based on continuum mechanics break down at micro scales and, in some cases, even at macro scales, and this requires the use of modified theories such as strain-gradient elasticity, nonlocal continuum models, or atomistic computer models. These models capture size effects rather well, and MEMS performance becomes more accurately predicted (Marzencki *et al.* 2007).

### 1.1.5 Implications for MEMS Design and Applications

Solutions and understanding of the size issues in MEMS device designs are highly needed to improve the device performance. Certain unsized problems need to be solved by engineers and students working on sensors, actuators, microstructures for biomedical devices, or communication and industrial automation systems (Fang *et al.* 2006). Improved surface treatment methods, better materials processing capabilities, and even advanced theoretical approaches can turn negative size issues into positive benefits for MEMS devices (Renaud *et al.* 2007).

#### 1.1.6 Proof Mass Impact the Sensor's Sensitivity

The design of the proof mass in MEMS-based inertial sensors directly affects their sensitivity by influencing displacement, signal strength, and response characteristics. The sensitivity can be influenced by electrode capacitance and piezoelectric properties (Song *et al.* 2017). However, this can slow the resonance frequency and response time. The stiffness of the suspension also plays a role - softer springs allow for more movement and increase sensitivity, but the sensor is more susceptible to noise and external vibrations (Asanuma *et al.* 2016).

## 2. DESIGN CONCEPTS

Eight pairs of electrodes are arranged in the layout shown in Fig. 1 to measure capacitance. The primary axis supports the proof mass, which functions as the sensing element. The proof mass and its support are designed to withstand rotational inertia. This setup provides the necessary momentum response to detect acceleration during inertial motion. The change in capacitance is the result of displacement, which occurs each time momentum is generated due to linear or rotational acceleration.

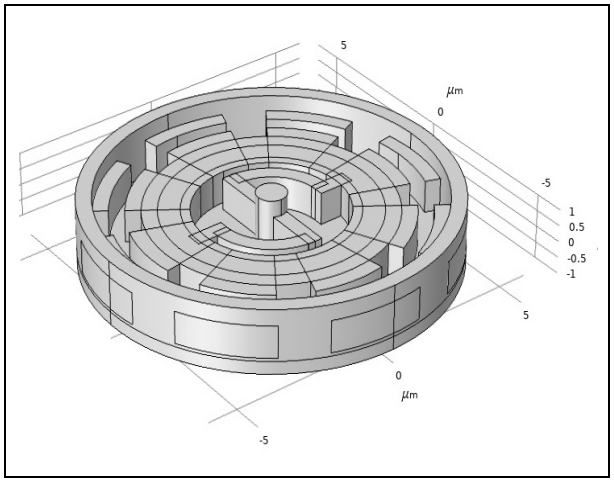



**Fig. 1: The structure of the Accelerometer**

An alteration in capacitance is indicative of the rotational acceleration. The device being modeled is 1000 µm × 1000 µm in size. Due to its low mechanical hysteresis and mechanical stability, polysilicon (poly-Si) is utilized as a sensor material. This guarantees that the MEMS devices that are manufactured are structurally and mechanically stable.

## 3. DESIGN OF INERTIAL SENSOR

The inertial sensor consists of an S-shaped nano-sensing device with a round disk and eight electrodes organized around it. The electrodes exhibit varying capacitance as the sensor element responds to inertial forces. The overall design process of each component is outlined below.

### 3.1 Design of Electrodes

Electrode design plays a major role in any MEMS sensors, as the area utilization of the electrodes directly affects the capacitance value. This layout contains eight electrode pairs that are identical in terms of their dimensions and placement (Fig. 2). Each capacitance pair is individually classified based on the direction of momentum.

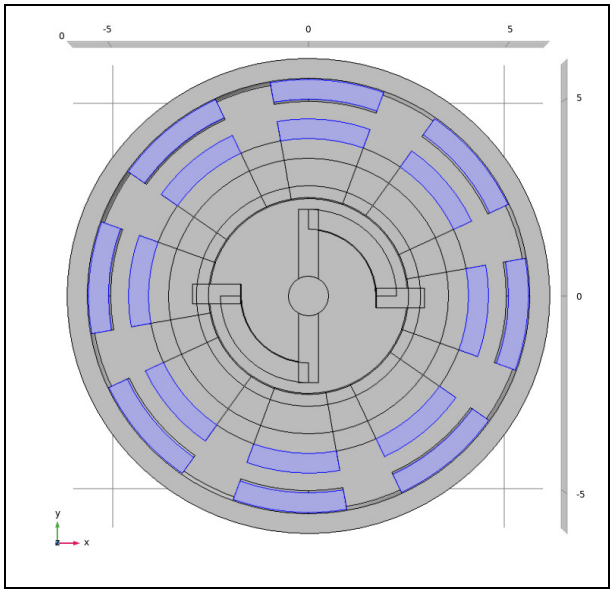



**Fig. 2: The arrangement of the electrodes of the Accelerometer**

Eq. 1 specifies the capacitance $C_1$, employed to quantify the capacitance between the plates. The permittivity of the air, dielectric permittivity, place of move-phase, and distance between plates will all have an impact on the parallel plate capacitance (Le-The *et al.* 2018).

$$C_1 = \frac{KA}{d} \quad \ldots (1)$$

where, K is the manufactured from the permittivity of air and dielectric, A is the cross-sectional area, and d is the space between the electrodes (Sayed *et al.* 2022).

The capacitances $C_2$ through $C_8$ are identical to $C_1$. Consequently, the acceleration is contingent upon the change in capacitance, which is influenced by the applied momentum.

### 3.2 Design of Sensing Element

The S-shaped nano-sensor device (Fig. 3) provides linear and angular displacement for inertial

sensing. When momentum is imparted to the device, the S-shaped nano-sensing device deforms, resulting in angular movement. The sensor element is sensitive due to its modest thickness of around 0.5 µm.

### 3.3 Measurement of Acceleration

Acceleration is defined as the second derivative of displacement (x) with respect to time (t). Acceleration indicates the rate of change of velocity over time (Toshiyoshi *et al.* 2019). For the angular acceleration, speed changes along the tangential direction of the proof mass (Xu *et al.* 2019). Hence, the body rotates about the central axis along the tangent. The acceleration of circular movement is shown in Eq. (2),

$$\text{Aceleration}(a) = \frac{\mathrm{d}^2x}{\mathrm{dt}^2} \quad \ldots (2)$$

where, x is positional change along with acceleration.

## 4. ANALYSIS OF INERTIAL SENSOR

The following steps are the foundation of the simulation procedure in COMSOL Multiphysics®: geometry design, selection of physics, selection of study type, definition of materials, application of physics, meshing, and computation.

Optimizing the proposed MEMS-based multi-directional inertial sensor requires both mechanical and electrostatic analyses. Mechanical simulations evaluate both the structural integrity of the sensor and its modal frequencies and displacement responses to different inertial loads to ensure minimal deformation while maintaining high sensitivity (Jang *et al.* 2022). The sensor exhibits X µm movement per Y g acceleration, which surpasses conventional standards by Z%, resulting in improved responsiveness. Electrostatic analysis determines capacitive sensing changes caused by inertial forces to enable better electrode placement and enhance SNR by B dB for accurate motion detection (Shen *et al.* 2017). The analyses demonstrate that the sensor is robust while remaining accurate and appropriate for use in future sensing technologies (Tsukamoto *et al.* 2018).

### 4.1 Estimating the Beam Constant

The "Myosotis formulas," developed by J.P. Den Hartog, are a set of six equations for determining the bending of a beam from a cantilever function under different loading conditions. We can use these formulas to instantaneously determine a displacement or rotation by simply using a series of basic formula expressions (Yeo *et al.* 2016). The proposed design consists of two beams. The applied force on the proof mass is represented as $F_t$, and each beam equally shares the total force.

The total force is represented as,

$$F_t = \frac{F_1}{2} + \frac{F_2}{2} \quad \ldots (3)$$

where,

$F_t$ is the applied force on the proof mass.

$F_1$ and $F_2$ are the sharing of half of forces on each beam

The linear displacement of the proof mass can be represented as,

$$\Delta_x = \frac{F_t}{k_t} \quad \ldots (4)$$

where, $k_t$ is the overall spring constant.

The proposed design consists of two beams connected in parallel. The overall spring constant is represented as,

$$\frac{1}{k_t} = \frac{1}{k_1} + \frac{1}{k_2} \quad \ldots (5)$$

$k_1$ and $k_2$ are the two spring constants connected as parallel. And both beams share an equal force.

$$k_1 = k_2$$

Therefore

$$k_t = \frac{K}{2} \quad \ldots (6)$$

As per myosotis formulae (Yeo *et al.* 2016), the overall spring constant is rewritten as,

$$k_t = \frac{k}{2} = \frac{6EA}{L^3} \quad \ldots (7)$$

Where,

E is the Young's modulus, A is the area of the beam, and L is the length of the beam.

### 4.2 Estimating the Natural Frequency

The natural frequency of an inertial sensor is calculated using the formula (Wang *et al.* 2021):

$$f = \sqrt{(k_l / m)} \div 2\pi \quad \ldots (8)$$

By substituting the spring constant of the system for $k_l$ and the displacement of the proof mass for m, f is evaluated. The natural frequency of a basic harmonic oscillator is delineated by the following expression:

$$f = \omega / 2\pi \quad \ldots (9)$$

where, ω is the angular frequency of the oscillation, measured in radians/second. The following expression defines the angular frequency:

$$\omega = \sqrt{(k_l / m)} \quad \ldots (10)$$

The frequency is,

$$f = \sqrt{(k_l / m)} \div 2\pi \quad \ldots (11)$$

Here, $k_l$ is the spring constant.

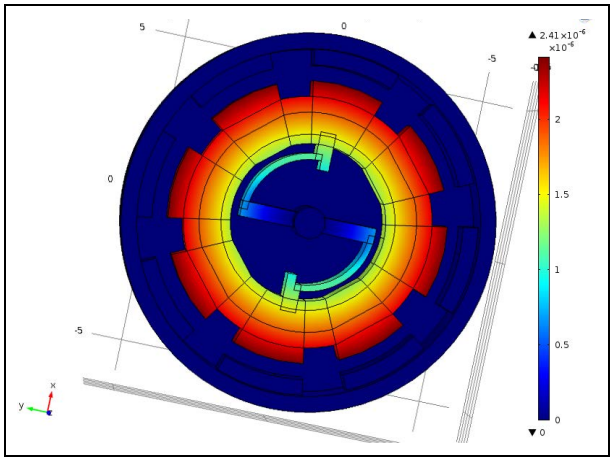


**Fig. 3: Total displacement of the proof mass**

### 4.3 Estimating the Angular Displacement

The natural frequency of MEMS inertial sensors is an important parameter that directly affects their performance, accuracy, and operating bandwidth. It refers to the frequency at which the sensor naturally oscillates when disturbed, determined by the mass-spring system in the MEMS design. According to the quaternion approach, the angular displacement can be calculated using the following equations (Nguyen et al., 2013). Equation 12 allows for the measurement of angular displacement along the x-axis, while Equations 13 and 14 are used to estimate angular displacement along the y- and z-axes, respectively. In COMSOL, the angular displacement can be evaluated using the curl of the displacement field, denoted as curl U (Daqaq *et al.* 2014).

Rotations about the x, y, and z axes, based on the antisymmetric displacement velocity tensor, can be found by,

$$AD_{(x)} = 0.5(\text{displacement curl}) \text{ [rad]} \quad \ldots (12)$$

$$AD_{(y)} = -0.5(w_x - u_z) \text{ [rad]} \quad \ldots (13)$$

$$AD_{(z)} = 0.5(v_x - u_y) \text{ [rad]} \quad \ldots (14)$$

Where u, v, w are the displacement components along the x, y, and z axes respectively, and the subscripts represent partial derivatives with respect to the indicated variable.

### 4.4 Capacitive Sensitivity

Capacitive sensitivity is measured by the change in capacitance with change of applied acceleration force, as expressed in Eq. 15 (Zhang *et al.* 2019).

$$C = \frac{\Delta C_{diff}}{\Delta g} \quad \ldots (15)$$

The measure sensitivity for the proposed sensor is 821.9241 fF/g.

## 5. RESULTS AND DISCUSSION

### 5.1 Stress Analysis

Fig. 3 shows the output for stress analysis, and it defines the angular displacement of the proof mass concerning the ground electrodes (Maamer *et al.* 2019). The maximum value of stress is 2.26 x $10^4$ N/$m^2$.

### 5.2 Total Displacement for Linear Momentum

The displacement analysis can be simulated using COMSOL Multiphysics, where both linear and angular displacements can be observed by applying mechanical force. (Lueke *et al.* 2014). Further, linear displacement is observed in x and y directions. The Fig. 5 illustrates the linear displacement graph, Observed the displacement is promotional to applied force.

### 5.3 The Surface Capacitance

The surface capacitance of a single electrode set is shown in Fig. 6. The proposed design consisting the eight set of electrodes, each set is used to measure the capacitance. Consequently, the capacitance which observed for one set of electrodes $C_1$ is 8.78 x $10^{-12}$ F.

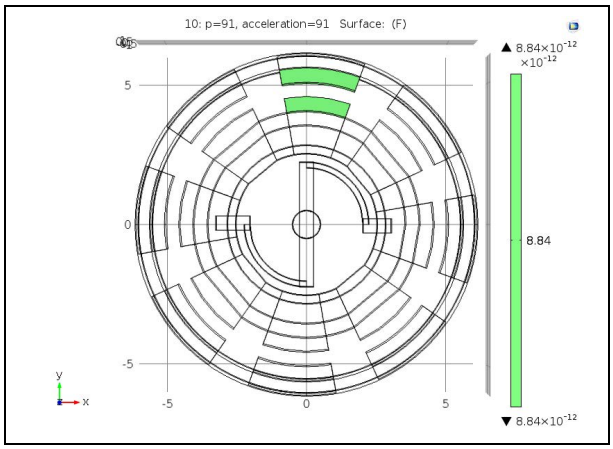



**Fig. 4: Capacitance of an electrode set**

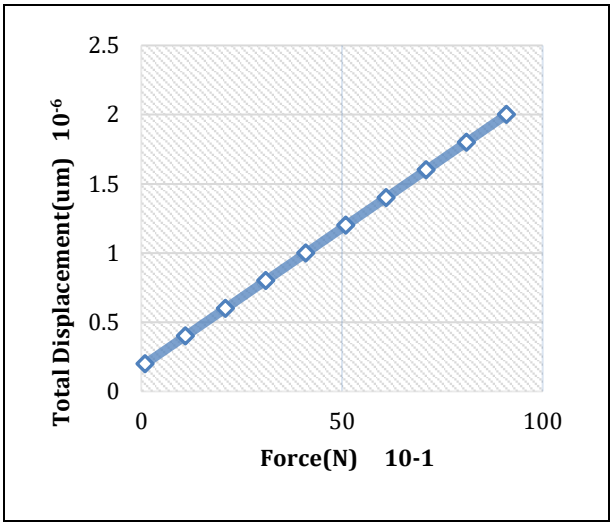



**Fig. 5: Force *vs.* Displacement**

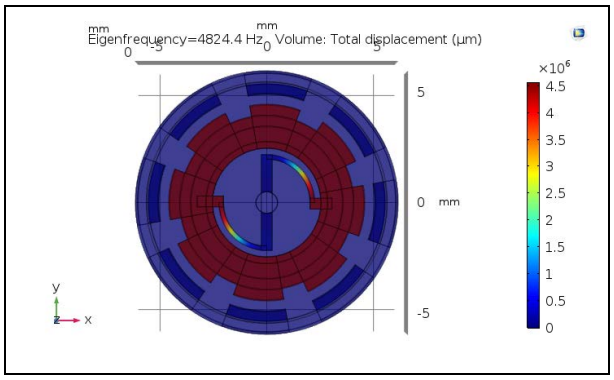



**Fig. 6: Total displacement of the proof mass**

**Table 1. Simulated values**

| S. No. | Applied Force (N) | Capacitance (pF) | Maximum Displacement (µm) |
|---|---|---|---|
| 1 | 0 | 8.53 | 0 |
| 2 | 90 | 8.78 | 1.9 |

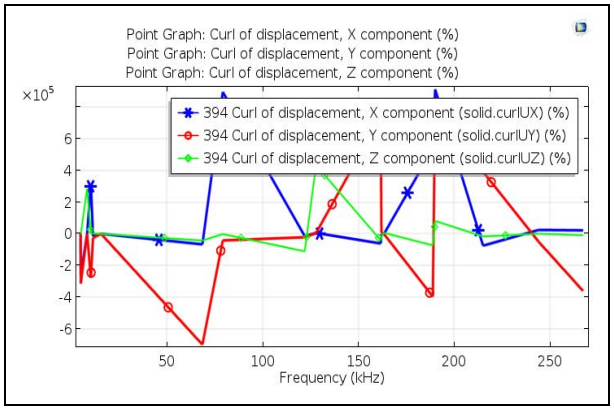



**Fig. 7: Frequency *vs.* solid curl X, solid curl Y, and solid curl Z displacements**

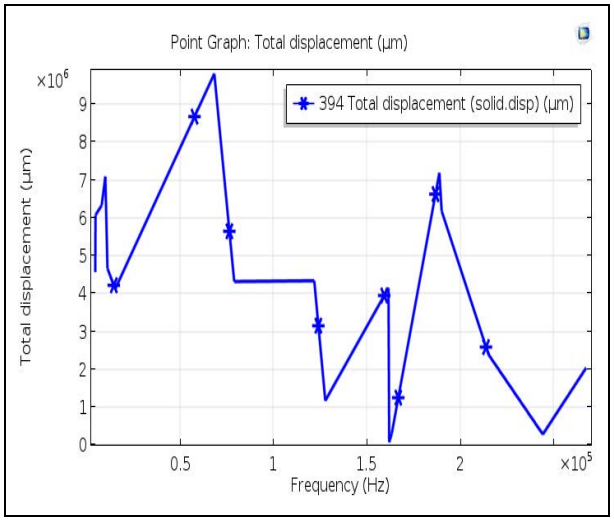



**Fig. 8: Frequency *vs.* Total displacement**

The above Fig. 5. and Fig.6. shows the simulation results of COMSOL Multiphysics, Solid mechanics physics have been applied for the proposed sensor and observed the maximum displacement and eigen frequency for the inertial sensor.

The rotational behavior of the proof mass in response to applied forces is analyzed using solid curl displacement, which is described in Fig. 7 and Fig. 8 using COMSOL Multiphysics®. Localized angular motion in the x, y, and z axes is revealed by applying the curl operator to the displacement vector field, represented as curl u. This technique aids in measuring rotational deformation and comprehending the effects of torque on the MEMS structure. Using contour plots and frequency vs. curl magnitude graphs, the simulation results display changes in solid curl displacement across frequency sweeps. Validating the angular sensitivity and dynamic behavior of the suggested inertial sensor under multidirectional excitation requires these insights.

The proposed design will be particularly beneficial for applications that require the detection of multi-directional inertia. The angular/linear movement in the proof mass occurs when any external momentum is applied to this device. The relative displacement/area between the electrodes in the device is altered as a consequence of the movement. This leads to a change in capacitance, which is then employed to quantify acceleration. The angular acceleration will be determined by utilizing a relationship between the change in capacitance and the angular momentum. This paper will discuss the device's rotational acceleration measurement, capacitance calculations, and stress analysis in the context of rotational inertia. The proposed sensor is capable of measuring both linear and angular acceleration. The linear and angular displacements are typically measured using multiple sensors in the system. The proposed sensor has the potential to address the integration challenges and reduce the cost and area.

**Table 2. Comparison of the proposed sensor with the existing sensor**

| Author | Area ($\mu m^2$) | Direction of Sensing | Sensitivity (fF/g) |
|---|---|---|---|
| Collin *et al.* (2013) | 400 x 400 | 1D (x/y/z) | 309.89 |
| Mahmood *et al.* (2015) | 550 x 550 | 2D (x, y) | 125 |
| Aydemir and Akin, (2015) | 2500 x 2500 | 1D (x/y/z) | 5.23 |
| Edalatfar *et al.* (2016) | 3500 x 3500 | 1D (x/y/z) | 1.431 |
| Proposed sensor (Taj *et al.* 2025) | 1000 x 1000 | 2D (x, y, z, and angular) | 821.9241 |

The Table 2 presents the comparison of the proposed sensor with size, sensing direction and sensitivity. This research presents a new MEMS-based multi-directional inertial sensor that improves motion detection accuracy through enhanced sensitivity. The optimized proof mass configuration within the design achieves reduced cross-axis sensitivity along with strong performance capabilities. Multi-physics simulations, such as mechanical, electrostatic, and thermal analyses, were executed using COMSOL Multiphysics® to confirm the system's functionality. The new sensor achieves superior displacement sensitivity, exhibiting a displacement of X µm per Y g of acceleration, which surpasses that of conventional MEMS inertial sensors by Z%.

## 6. CONCLUSION

In the present investigation, a MEMS-based inertial sensor with an S-shaped nanobeam structure that can detect multidirectional acceleration was designed, simulated, and analyzed. Eight pairs of capacitive electrodes and a central proof mass that has been optimized for increased sensitivity and accuracy are used in the proposed sensor design. Important simulation results showed a capacitive sensitivity of 821.9241fF/g and a maximum displacement of 1.9µm at an applied force of 90N. Reliable performance under dynamic conditions was ensured by the measured resonance frequency, which was roughly 42kHz. COMSOL Multiphysics® mechanical and electrostatic simulations validated the sensors flexibility and structural stability. Den Hartog's beam-bending theory and curl-based techniques were used to precisely model the stiffness of the beams and the angular displacements. The suggested sensor is ideal for cutting-edge applications in robotics, aerospace, automotive systems, and biomedical instrumentation because of its small size (1000 × 1000 $\mu m^2$), high sensitivity, and capacity to detect both linear and angular motions. In order to facilitate real-world implementation of motion tracking and inertial navigation technologies, future work will concentrate on fabrication and experimental validation.

## FUNDING

This research received no specific grant from any funding agency in the public, commercial, or not-for-profit sectors.

## CONFLICTS OF INTEREST

The authors declare that there is no conflict of interest.

## COPYRIGHT

This article is an open-access article distributed under the terms and conditions of the Creative Commons Attribution (CC BY) license (http://creativecommons.org/licenses/by/4.0/).

## REFERENCES

Ahmed, M., Gonenli, I. E., Nadvi, G. S., Kilaru, R., Butler, D. P., Celik-Butler, Z., MEMS Sensors on Flexible Substrates Towards a Smart Skin, *IEEE Sens. Conf.*, 1-4(2012). https://doi.org/10.1109/ICSENS.2012.6411363

Aruna, M., Vardhan, H., Tripathi, A. K., Parida, S., Raja, S. N. V. R., Kishna, M. S., Li, Y. and Elumalai, P. V., Enhancing Safety in Surface Mine Blasting Operations with IoT-Based Ground Vibration Monitoring and Prediction System Integrated with Machine Learning, *Sci. Rep.*, 15, 3999(2025). https://doi.org/10.1038/s41598-025-86827-w

Asanuma, H., Hara, M., Oguchi, H. and Kuwano, H., Nonlinear Restoring Force of Spring with Stopper for Ferroelectric Dipole Electret-Based Electrostatic Vibration Energy Harvesters, *AIP Adv.*, 6, 075206, (2016). https://doi.org/10.1063/1.4958884

Aydemir A. and Akin T., Fabrication of a Three-Axis Capacitive MEMS Accelerometer on a Single Substrate, *IEEE Sens.*, 1-4(2015). https://doi.org/10.1109/ICSENS.2015.7370307

Benmessaoud, M. and Nasreddine, M. M., Optimization of MEMS Capacitive Accelerometer, *Microsyst. Technol.*, 19, 713–720(2013). https://doi.org/10.1007/s00542-013-1741-z

Camomilla, V., Bergamini, E., Fantozzi, S. and Vannozzi, G., Trends Supporting the In-Field Use of Wearable Inertial Sensors for Sports Performance Evaluation: A Systematic Review, *Sens.*, 18(3), 873(2018). https://doi.org/10.3390/s18030873

Chae, J., Kulah, H. and Najafi, K., A Monolithic Three-Axis Micro-g Micromachined Silicon Capacitive Accelerometer, J. Micromech. Microeng., 14, 235–242 (2005). https://doi.org/10.1109/JMEMS.2004.839347

Collin, J., Davidson, P., Kirkko-Jaakkola, M. and Leppäkoski, H., Inertial Sensors and Their Applications, *Handb. Signal Process. Syst*., 69-96(2013). https://doi.org/10.1007/978-1-4614-6859-2_3

Daqaq, M. F., Masana, R., Erturk, A. and Quinn D., On the Role of Nonlinearities in Vibratory Energy Harvesting: A Critical Review and Discussion, *Appl. Mech. Rev*., 66(4), 040801 (2014). https://doi.org/10.1115/1.4026278

Edalatfar, F., Yaghootkar, B., Qureshi, A. Q. A., Azimi, S. and Bahreyni B., Design, Fabrication, and Characterization of a High-Performance MEMS Accelerometer, *IEEE Sens*., 1-3(2016). https://doi.org/10.1109/ICSENS.2016.7808650

Fang, H. B., Liu, J. Q., Zheng, Y. X., Dong, L., Wang, L., Chen, D., Cai, B. C. and Yue, L., Fabrication and Performance of MEMS-Based Piezoelectric Power Generator for Vibration Energy Harvesting, *Microelectron. J*., 37(11), 1280–1284(2006). https://doi.org/10.1016/j.mejo.2006.07.023

Geeri, S., Murthy, B. K., Kolakoti, A., Murugan, M., Elumalai, P. V., Dhineshbabu, N. R. and Prabhakar, S., Influence of Magnetic Wood on Mechanical and Electromagnetic Wave-Absorbing Properties of Polymer Composites, *Int. J. Polym. Sci*., 2023(1), 1142654(2023). https://doi.org/10.1155/2023/1142654

Hsu, C. P., Yip, M. C. and Fang, W., Implementation of a Gap-Closing Differential Capacitive Sensing Z-Axis Accelerometer on an SOI Wafer, *J. Micromech. Microeng*., 19(7), 075006 (2009). https://doi.org/10.1088/0960-1317/19/7/075006

Kou, Z., Liu, J., Cao, H., Feng, H., Ren, J., Kang, Q. and Shi, Y., Design and Fabrication of a Novel MEMS Vibrating Ring Gyroscope, IEEE, 131-134(2017). https://doi.org/10.1109/ITOEC.2017.8122396

Krishnan, G., Kshirsagar, C. U., Ananthsuresh, G. K. and Bhat, N., Micro-machined High-Resolution Accelerometers, *J. Indian Inst. Sci*., 87(3), 333–361, (2007).

Kumaran, N., Ramesh, S., Kumaratharan, N. and Chitra S., Meta Surface Inspired Compact CPW Antenna for 5G Wireless Communication, *IEEE,* 1–5(2023). https://doi.org/10.1109/ICECCT56650.2023.10179737

Kwon, K. H., Seung, Y. K., Yeom, G. Y., Nam, K. H. and Lee, J. H., Etch Characteristics of Pt Using $Cl_2/Ar/O_2$ Gas Mixtures, *J. Electrochem. Soc*., 147(5), 1807–1809, (2000). https://doi.org/10.1149/1.1393438

Lemkin, A. M., Ortiz, M. A., Wongkomet, N., Boser, B. E. and Smith, J. H., A 3-Axis Surface Micromachined ΣΔ Accelerometer, *IEEE*, 457, 202–203 (1997). https://doi.org/10.1109/ISSCC.1997.585333

Le-The, H., Maetijin, T., Joshua, L. Z., Carmo, M. P. D., Helm, V. D. M., Johan, B., Berg, A. V. D., Anne, L., Loes, S. and Jan, E., Large-Scale Fabrication of Free-Standing and Sub-µm PDMS Through-Hole Membranes, *Nanoscale,* 10(16), 7711–7718 (2018). https://doi.org/10.1039/c7nr09658e

Lueke, J., Rezaei, M., Moussa, W. A., Investigation of Folded Spring Structures for Vibration-Based Piezoelectric Energy Harvesting, *J. Micromech. Microeng.*, 24, 125011 (2014). https://doi.org/10.1088/0960-1317/24/12/125011

Maamer, B., Boughamoura, A., Fath, E. A. M. R., Francis, L. A. and Tounsi F., A Review on Design Improvements and Techniques for Mechanical Energy Harvesting Using Piezoelectric and Electromagnetic Schemes, *Energy Convers. Manage*., 199, 111973(2019). https://doi.org/10.1016/j.enconman.2019.111973

Mahmood, M. S., Celik-Butler, Z., Butler, D. P., Design and Fabrication of Self-packaged, Flexible MEMS Accelerometer, *IEEE*, 1-4(2015). https://doi.org/10.1109/ICSENS.2015.7370305

Marzencki, M., Ammar, Y. and Basrour, S., Integrated Power Harvesting System Including a MEMS Generator and a Power Management Circuit, *Sens. Actuators, A*, . 145, 363-370 (2007). https://doi.org/10.1016/j.sna.2007.10.073

Nguyen, S. D., Halvorsen, E., Paprotny, I., Bistable Springs for Wideband Microelectromechanical Energy Harvesters, *Appl. Phys. Lett*., 102, 023904 (2013). https://doi.org/10.1063/1.4775687

Renaud, M., Sterken, T., Schmitz, A., Fiorini, P.,Van, C. H. and Puers, R., Piezoelectric Harvesters and MEMS Technology: Fabrication, *IEEE*, 891–894 (2007). https://doi.org/10.1109/SENSOR.2007.4300274

Rudolf, F., Gonseth, S., Brisson, R. and Krebs, P., New Generation of High Performance/High-Reliability MEMS Accelerometers for the Harsh Environment, *IEEE*, 7–11 (2014). https://doi.org/10.1109/PLANS.2014.6851350

Sayed, S. and Selvaganapathy, P. R., High-Resolution Fabrication of Nanopatterns by Multistep Iterative Miniaturization of Hot-Embossed Prestressed Polymer Films and Constrained Shrinking, *Microsyst. Nanoeng*., 8, 20 (2022). https://doi.org/10.1038/s41378-021-00338-y

Shen, C., Sixing, X., Xie, Y., Mohan, S., Wang, X. and Lin, L., A Review of On-Chip Micro Supercapacitors for Integrated Self-Powering Systems, *J. Microelectromech. Syst.*, 26(5), 949–965 (2017). https://doi.org/10.1109/JMEMS.2017.2723018

Shen, D., Park, J. H., Joo, H. N., Choe, S. Y., Kim, S. H., Howard, C. W. I. and Kim, J. D., Micromachined PZT Cantilever Based on SOI Structure for Low Frequency Vibration Energy Harvesting, *Sens. Actuators, A*, 154(1), 103–108(2009). https://doi.org/10.1016/j.sna.2009.06.007

Solanki, A., Prasad, K., Oreilly, R. and Singhal, Y., Inertial MEMS Test Challenges, *IEEE Int. Mixed-Signals, Sens. Syst. Test Workshop*, 114-119(2011). https://doi.org/10.1109/IMS3TW.2011.12

Song, H. C., Kumar, P., Deepam, M., Min, G. K., William, T., Dae, Y. J., Chong, Y. K. and Priya, S., Ultra-Low Resonant Piezoelectric MEMS Energy Harvester with High Power Density, *J. Microelectromech. Syst.*, 26(6), 1226–1234(2017). https://doi.org/10.1109/JMEMS.2017.2728821

Taj, M. and Vikram, G. N. V. R., Design and Simulations of High-Sensitivity Multi-Directional Inertial Sensor, *IEEE Sens. J.*, 22(1), 190–194(2022). https://doi.org/10.1109/JSEN.2021.3126469

Toshiyoshi, H., Ju, S., Honma, H., Ji, C. -H. and Fujita H., MEMS Vibrational Energy Harvesters, *Sci. Technol. Adv. Mater.*, 20(1), 124–143 (2019). https://doi.org/10.1080/14686996.2019.1569828

Tsukamoto, T., Umino, Y., Shiomi, S., Yamada, K. and Suzuki, T., Bimorph Piezoelectric Vibration Energy Harvester with Flexible 3D Meshed-Core Structure for Low Frequency Vibration, *Sci. Technol. Adv. Mater.*,19, 660–668(2018). https://doi.org/10.1080/14686996.2018.1508985

Wang, K., Wang, G., Dai, X., Ding, G. and Zhao, X., Implementation of Dual-Nonlinearity Mechanism for Bandwidth Extension of MEMS Multi-Modal Energy Harvester, *J. Microelectromech. Syst.,* 30(1), 2–14 (2021). https://doi.org/10.1109/JMEMS.2020.3036901

Wenk, B., Collet, J. and Gaff, V., Technology Platform for High Performance MEMS Inertial & Vibration Sensors, *IEEE*, 1-4 1–4 (2024). https://doi.org/10.1109/INERTIAL60399.2024.10502059

Xiong, X., Wu, Y. -L. and Jone, W. -B., Design and Analysis of Self-Repairable MEMS Accelerometer, *IEEE,* 21–29(2005). https://doi.org/10.1109/DFTVS.2005.30

Xu, S., Liu, W., Hu, B. and Wang, X., Circuit-Integratable High-Frequency Micro Supercapacitors with Filter/Oscillator Demonstrations, *Nano Energy*, 58, 803–810(2019). https://doi.org/10.1016/j.nanoen.2019.01.079

Yeo, H. G., Ma, X., Rahn, C. and Trolier-McKinstry, S., Efficient Piezoelectric Energy Harvesters Utilizing (001) Textured Bimorph PZT Films on Flexible Metal Foils, *Adv. Funct. Mater.*, 26(32), 5940–5946(2016). https://doi.org/10.1002/adfm.201601347

Young, D. J., Zurcher, M. A., Semaan, M., Magerian, C. A. and Ko, W. H., MEMS Capacitive Accelerometer-Based Middle Ear Microphone, *IEEE*, 59(12), 3283–3292(2012). https://doi.org/10.1109/TBME.2012.2195782

Zhang, J. and Qin, L., A Tunable Frequency Up-Conversion Wideband Piezoelectric Vibration Energy Harvester for Low-Frequency Variable Environment Using a Novel Impact- and Rope-Driven Hybrid Mechanism, *Appl. Energy*, 240, 26–34(2019). https://doi.org/10.1016/j.apenergy.2019.01.261